Bull. Mater. Sci. (2018) 41:86
https://doi.org/10.1007/s12034-018-1592-4

Bio-inspired AgNPs, multilayers-reduced graphene oxide and graphite nanocomposite for electrochemical H_2O_2 sensing

RAJ KUMAR DAS, SNIGDHA SAHA, VENKATANARASIMHA RAO CHELLI and ANIMES KUMAR GOLDER*
Department of Chemical Engineering, Indian Institute of Technology Guwahati, Guwahati 781039, India
*Author for correspondence (animes@iitg.ernet.in)

MS received 11 June 2017; accepted 10 October 2017; published online 29 May 2018

Abstract. A bio-mediated route for the synthesis of silver nanoparticles (AgNPs) is an area of interest in research of many scientists, and this work aims to study the electrocatalytic activity of these particles during electrochemical sensing of H_2O_2 in a phosphate buffer media. The composite electrodes were fabricated using nearly spherical AgNPs and reduced graphene oxide (rGO) with the graphite (99.999% purity) support made of graphite paste. Graphene oxide (GO) was first synthesized using the modified Hummers method followed by rGO synthesis by chemical reduction of GO. rGO is consisting of about nine layers of rGO sheets of a wrinkled surface morphology with an intensity ratio of D to G band (I_D/I_G) of 1.17 and an interplanar *d*-spacing of 0.36 nm as evidenced by HRTEM micrograph. There was about 10 times increase in the cell current with the AgNPs-impregnated composite–electrode compared to without AgNPs impregnation, and an overpotential of H_2O_2 reduction was found to be −1.373 V with a detection limit of 19.04 μM and 95.3% electrode stability with the graphite–rGO–AgNPs composite electrode. A nafion membrane cast on the rGO–AgNPs prevented the leakage of this composite from the electrode surface. The interference of various electroactive compounds on the amperometric response of the graphite–rGO–AgNPs electrode was also investigated.

Keywords. Electrochemical sensor; H_2O_2 detection; silver nanoparticles; reduced graphene oxide.

1. Introduction

H_2O_2, a reactive oxygen species, has numerous applications in biomedical, clinical, pharmaceutical, food production and pulp and paper bleaching [1]. It is used as a mediator in many organic compound synthesis reactions and liquid-based fuel cells [2]. Moreover, H_2O_2 is considered as an environment-friendly chemical as it breaks down into water and oxygen after the reaction. In water treatment, H_2O_2 is used mostly as a precursor of hydroxyl radicals ($HO^{\bullet}$) generation (2.8 V *vs.* normal hydrogen electrode) for a quick and effective decomposition of organic and inorganic compounds [3,4].

Therefore, a sensitive, reliable, rapid and low-cost method of H_2O_2 determination is imperative. The electrochemical methods owe the advantages of easy fabrication, quick sensing, low sample volume, low detection limit and high selectivity [5]. However, the direct redox reaction of H_2O_2 at typical solid electrodes is a slow process, and needs a high overpotential. This problem can be overcome by modifying the bare electrode with the suitable electrocatalysts, so that the high overpotential for H_2O_2 reduction is decreased [1].

The enzyme-based electrochemical sensors are employed for faster electron transfer and to lower the reduction potential. Horseradish peroxidase [6], cytochrome C [7], haemoglobin [8] and myoglobin [9] are tested extensively for the fabrication of electrochemical biosensor for H_2O_2 detection due to high sensitivity and selectivity even with the presence of interfering components. However, the enzyme-based electrodes suffer from instability, high-enzyme cost and complex immobilization technique. The enzyme activity is also significantly dependent on temperature, media pH and chemical toxicity [1].

To solve the problems related to H_2O_2 detection by the enzymatic electrochemical methods, the non-enzymatic electrodes mediated with noble metals [10] and metal oxides [11], metal alloys [12] and metal NPs [13] as electrocatalysts are developed.

Nanoparticles (NPs) possess unique characteristic properties than its bulk parts [14]. Considerable research initiatives were taken up in the recent past on bio-mediated processes for the synthesis of NPs of noble metal ions like Ag^+, Au^+ and Pt^+. It primarily explores the reduction efficiency of (bio)organic reducing agents found in renewable and natural materials like microbes [15], algae [16], fungi [17], and plant and plant-based extracts [18]. Moreover, the bio-mediated processes could produce NPs of precise size and shape, and

Electronic supplementary material: The online version of this article (https://doi.org/10.1007/s12034-018-1592-4) contains supplementary material, which is available to authorized users.

also the particles could be free of contaminant [19]. However, the implication of bio-(mediated) synthesized metal NPs as electrocatalysts for the electrochemical sensing is almost non-existent.

Moreover, to enhance the sensitivity further, the electrodes are impregnated with the materials such as reduced graphene oxide (rGO), which exhibits electrocatalytic activity towards the analyte [20]. rGO has a two-dimensional planar carbon nanosheets composed of a single layer of sp^2 carbon atoms, which are densely packed in a honeycomb lattice of carbon [21]. rGO possess a tremendously high electron mobility even in the order of 200,000 $cm^2\ V^{-1}\ s^{-1}$, and the hole and electron mobilities are almost similar, which is also temperature-independent between 10 and 100 K. Single layer rGO exhibits the thermal conductivity as high as 3000 $W\ m^{-1}\ K^{-1}$ [22]. Therefore, rGO/metal–nanocomposites have attracted a considerable attention in electrocatalysis and electrochemical sensor development [22] owing to excellent electrical and thermal conductivities, remarkably high carrier mobility and density, and outstanding stability.

In this work, nearly spherical silver nanoparticles (AgNPs) were used as electrocatalysts, which were synthesized by a bio-mediated route using the aqueous extract of Chayote, the fruits of a perennial climber. Graphene oxide (GO) synthesized by the improved Hummers method was reduced to rGO using hydrazine hydrate. The composite electrodes were fabricated by impregnating rGO or rGO–AgNPs with the graphite (Gr) support made of graphite paste. The composite materials were adequately characterized using both the physiochemical and structural methods such as Raman and Fourier transform infrared (FTIR) spectroscopies, thermogravimetric analysis (TGA), X-ray diffraction (XRD), and transmission electron microscopy (TEM), scanning electron microscopy (SEM) and atomic force microscopy (AFM). The electrodes were screened based on the cyclic voltammetric response for H_2O_2 reduction, and then, the amperometric analysis was carried out over a wide concentration range of the analyte. The reproducibility, repeatability and selectivity of H_2O_2 detection using the Gr–rGO–AgNPs composite electrode was also tested in the presence of various electroactive chemicals.

2. Methods and materials

2.1 *Reagents*

Graphite power (<45 μm, 99.999%) used for GO and rGO syntheses was procured from Sigma-Aldrich, St. Louis, USA. Sulphuric acid (H_2SO_4, assay 95–98%), sodium hydroxide pellets (NaOH, assay min 98%), potassium chloride (KCl, assay min 99.5%) and orthophosphoric acid (H_3PO_4, assay min 98%) were purchased from Merck, Mumbai, India. Three molar KCl was used as the filling solution of the reference electrode (Ag/AgCl). Hydrochloric acid (HCl, assay min 35%), potassium permanganate ($KMnO_4$, assay min 99%), hydrogen peroxide (H_2O_2, assay min 30%) and hydrazine hydrate (N_2H_5OH, assay 80%) were purchased from LOBA Chemie, Mumbai, India. Milli-Q water (Millipore, USA, model: Elix 3) was used for the dilution and solution preparation. All the reagents and chemicals were of the analytical grade used as received without further purification. The phosphate buffer (pH 6.74) was prepared using NaH_2PO_4 and Na_2HPO_4 (Merck, Mumbai, India). Absolute ethanol (assay 99.9%) (Changshu Yangyuan Chemicals, China), glacial acetic acid (99–100%), glucose (assay 99.4%) (Merck, Mumbai, India), ascorbic acid (assay 99–100.5%) (LOBA Chemie, Mumbai, India), uric acid (assay ≥99%) (Sigma Aldrich, Bangalore, India) and dopamine hydrochloride (assay 98%) (Sigma Aldrich, Bangalore, India) were used as the interfering chemicals in the amperometric studies.

2.2 *Preparation of rGO*

2.2a *Synthesis of GO from graphite flakes*: GO is non-conductive and hydrophilic in nature. Hummers proposed a method by using $KMnO_4$ and $NaNO_3$ in concentrated H_2SO_4 for the synthesis of GO from graphite [23]. The improved Hummer's method excluded the use of $NaNO_3$, and increased the amount of $KMnO_4$, where the mixture of H_2SO_4 and H_3PO_4 improved the efficiency of the oxidation process. This improved method provides a greater amount of hydrophilic GO [24].

Herein, GO was synthesized by using the improved Hummer's method. In a typical synthesis experiment, 1 g graphite was added into the mixture of 23 ml 98% H_2SO_4 and 5 ml H_3PO_4 under continuous stirring. The mixture was kept below 5°C in an ice bath. Then, 5 g $KMnO_4$ was added to this mixture. $KMnO_4$ was added slowly in parts to keep the reaction temperature below 20°C. The agitation of the reaction mixture was continued for 30 min, and the mixture turned into purple brownish. The mixture was then heated to 40°C, and stirred for 12 h. It was cooled to room temperature, and 75 ml H_2O was added followed by 10 ml H_2O_2 (30%). The mixture turned into pale yellow colour.

It was then allowed to settle and the supernatant was decanted. The residue was first rinsed with 100 ml HCl (30%) to remove trace metals such as Mn^{2+}, and then repeatedly washed with hot water (∼ 60°C) till pH of the washout solution reached to 7. This whole process was carried out by centrifugation at 4000 rpm for 15 min followed by the removal of washout solution every time. The solid obtained after the simple filtration (0.45 μm) was vacuum-dried overnight at 50°C. The schematic diagram for the synthesis of GO is shown in figure S1 of the supplementary material.

2.2b *Synthesis of rGO from GO*: There are several methods for the rGO synthesis. In this work, rGO was prepared by reducing GO by hydrazine hydrate. One gram GO was dispersed in 200 ml H_2O in a conical flask for 1 h of ultrasonication (UC-02, Jeiotech Instruments, Korea) to have a homogenous dispersion. Then, 8 ml of hydrazine hydrate solution (80%) was added, and heated to 95°C for 24 h with

the open reflux. The product was filtered, washed with 5 × 100 ml deionized water and 5 × 100 ml ethanol, and then dried at 60°C. The steps involved in the synthesis of rGO is schematized in figure S2 of the supplementary material.

2.2c *AgNPs*: Chayote (also known as *Sechiumedule*) is an herbaceous perennial climber, and it contains a lot of natural antioxidants and ascorbic acids along with polyphenolic compounds, like flavonoids, phenylalanine and tyrosine [25,26]. The equal volume (30 ml each) of both Chayote extract and 1 mM $AgNO_3$ solution (pH 5.8) were mixed under constant stirring at 320 rpm for 24 h. The residue was repeatedly washed and dried at 90 ± 5°C in a hot-air oven for 12 h. The dried particles termed as AgNPs were kept in an air tight container and used for the subsequent analyses and tests. AgNPs used had an average particle size of 46 nm. The detailed synthesis methodology and characterization of AgNPs are reported in an earlier publication from the same research group [25,26]. The schematic diagram for the synthesis of AgNPs is illustrated in figure S3 of the supplementary material.

2.3 *Fabrication of rGO/AgNPs electrode*

It is well known that AgNPs exhibit a high catalytic activity for the reduction of H_2O_2 [27]. Five hundred milligrams of graphite sample and 0.75 g paraffin wax were mixed uniformly with 0.65 g rGO and 0.1 g AgNPs at a temperature of 60°C [28]. The mixture was put into a rectangular mould, and a copper wire (5.96×10^7 S m^{-1} at 20°C) was inserted in the centre. The electrode (Gr–rGO–AgNPs) was allowed to cool to room temperature. The electrochemical surface area of the electrode was 3.5 cm^2. Pt and Ag/AgCl were used as the counter and reference electrodes, respectively. Gr–rGO electrode was fabricated following the same procedure and composition, however, without AgNPs. The schematic diagram for the fabrication of G–rGO–AgNPs electrode is shown in figure S4 of the supplementary material.

2.4 *Characterization techniques*

Laser micro-Raman system (LabRam HR, Horiba JobinVyon, Japan) with 633 nm laser excitation beam was used to record the Raman spectra in the range of 900–3000 cm^{-1}. FTIR (IR affinity-1, Shimadzu, Japan) was carried out to identify the functional groups present in graphite, GO and rGO. KBr dried for 2 h at 110°C was used for the background correction. A small amount of sample was mixed with dried KBr in a mortar pestle for the pelletization to obtain the FTIR spectra for the wavelength range from 4000 to 500 cm^{-1}. XRD pattern was obtained to analyse the crystal structure of the specimens for the 2θ angle between 5 and 60° (D8-Advance, Bruker, Germany) with CuKα radiation of 0.15418 nm. Thermal gravimetric analyzer (TGA 851^e/LF/1100°C, Mettler Toledo, Switzerland) was used to check the thermal stability of the material between 30 and 800°C with an incremental rate of 10°C min^{-1}. TEM (JEM 2100, Jeol, USA) was used to study the morphology of the electrode material. One hundred milligrams of specimen was added in 20 ml ethanol and sonicated for 20 min in the ultrasonic bath to disperse individual particles. A digital pH meter (pH 700, Eutech Instruments, Malaysia) was employed for the measurement of pH of the electrolyte solution.

2.5 *Electrochemical studies*

Cyclic voltammograms (CV) were obtained in a 220 ml capacity undivided three-electrode cell with 185 ml analyte solution containing 0.2 M phosphate buffer (pH 6.74) with an initial amount of 1 mM H_2O_2. N_2 purging was continued for 20 min before the beginning of the experiment at 1.2 l min^{-1}. The scanning was performed at 20 mV s^{-1} using a potentiostat (AUTOLAB 302N, MetrohmAutolab B.V, The Netherlands). Graphite and the fabricated Gr–rGO and Gr–rGO–AgNPs electrodes were employed as the working electrodes, Pt as the counter and Ag/AgCl (3 M KCl) as the reference electrodes were used. All the experiments were carried out at the ambient temperature.

The amperometric test of H_2O_2 sensing was carried out following the same procedure, but at a fixed potential of −0.21 V *vs.* Ag/AgCl. An equal amount of 1 mM H_2O_2 was added to the analyte solution at every 50 s for a total test period of 1000 s. For the interference studies, after 200 s, acetic acid, ascorbic acid, glucose, uric acid, dopamine and ethanol were added one after the another in place of H_2O_2 with the same time interval and concentration of H_2O_2.

3. Results and discussion

3.1 *Characterization of precursors*

The Raman spectroscopy is used to characterize the carbonaceous materials for distinguishing the ordered and disordered carbon structures. The Raman spectra of graphite, GO and rGO are shown in figure 1. One of the in-plane vibrational modes of graphite is strongly Raman active, which was found at 1522 cm^{-1} (G-peak). There was also a broad peak (2D) at 2700 cm^{-1}. The spectrum of GO showed a typical D-peak at 1360 cm^{-1} and G-peak at 1601 cm^{-1}. The D- and G-peaks appeared at 1358 and 1608 cm^{-1} for rGO. The D-peak is due to the lattice motion away from the centre of the Brillouin zone, and its presence indicates the defects and edges in GO and rGO. The main defects in GO include oxygen groups such as carboxyl, carbonyls, hydroxyl and epoxy groups. The residual and vacancies become the main defects of rGO, once these groups are removed. The G-peak is the main spectral feature of rGO-like material derived from the in-plane motion of the carbon atom [29].

The D-peak of GO has a high intensity (I), which is attributed to the presence of functional groups. However, the D-intensity of rGO is still high even after the reduction (figure 1). This may be because hydrazine can reduce the

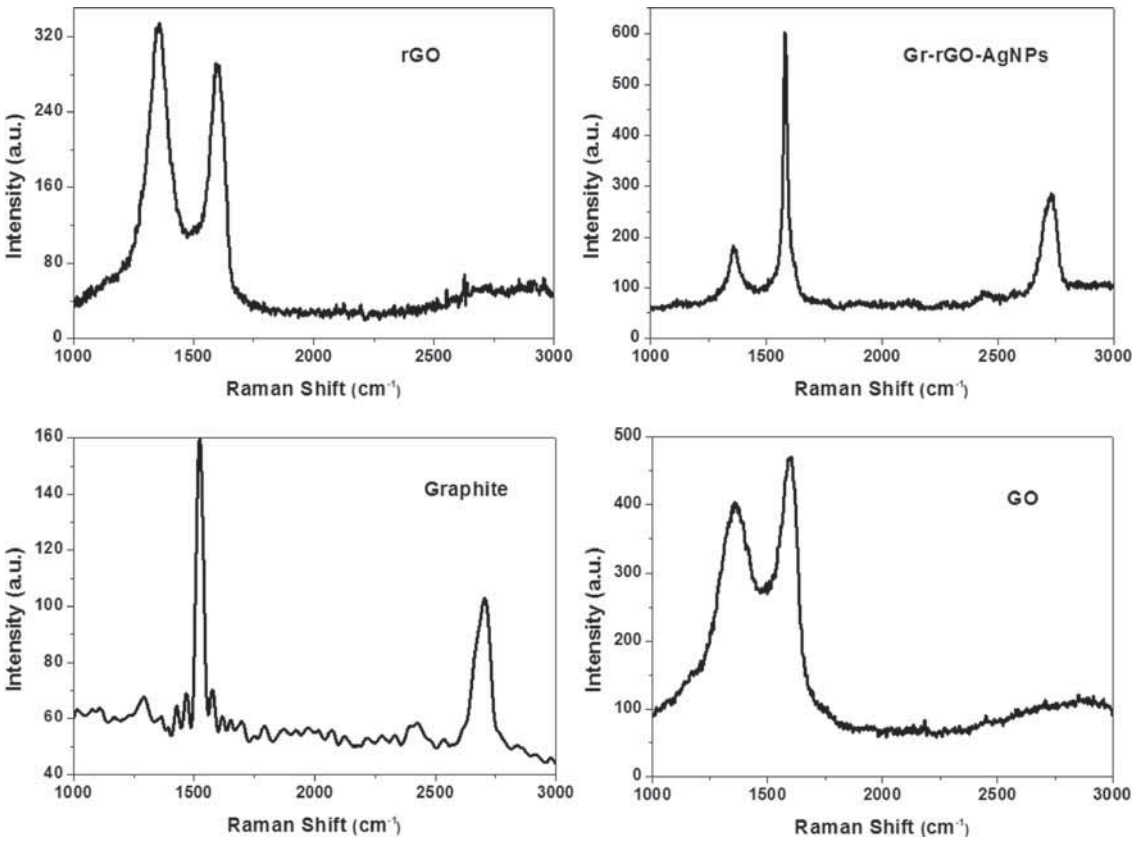

Figure 1. Raman spectra of graphite, synthesized GO and rGO.

carbonyl and carboxyl functional groups only. The shift of G-peak from 1601 to 1608 cm^{-1} is attributed to the decrease in the layer of GO particle or the exfoliation of particles, which depends on the degree of oxidation of graphite and more GO sheet can be formed [29].

The 2D-peak was observed at 2881 cm^{-1} and the band-shift and its shapes are correlated with the number of rGO layers. This is mainly because of the multilayers rGO and the shape of 2D band is different from that in the single-layer rGO. The 2D band in the single-layer rGO is much more intense and sharper as compared to the 2D band in multilayers rGO. Therefore, from the spectrum of rGO, it can be concluded that a multilayer rGO was synthesized. The composite material (Gr–rGO–AgNPs) was scrapped out from the electrode surface. It exhibited a weak D-peak at 1364.04 cm^{-1} and a strong G-peak at 1581.44 cm^{-1} more of GO and rGO. A 2D-peak appeared at 2734 cm^{-1} was the characteristic broad peak of graphite. No Raman shift was found for AgNPs. The intensity ratio of D to G band (I_D/I_G of GO was 0.85, and that of rGO was 1.17. The change in the ratio is due to the presence of unrepaired defect after the removal of oxygenated functional groups. The ratio is consistent with other chemical reduction processes [30].

Figure 2 shows the FTIR spectra of graphite, GO and rGO sheet. The graphite spectrum illustrates O–H broad

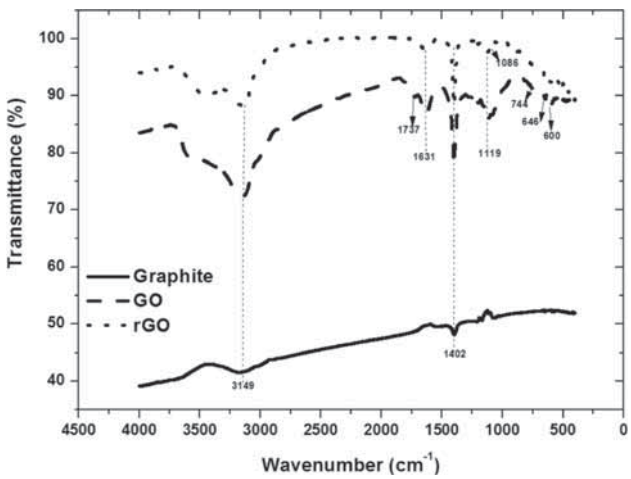

Figure 2. FTIR spectra of graphite, GO and rGO.

peak at 3149 cm^{-1} resulting from intercalated water and C–C stretched aromatic ring at 1402 cm^{-1}. The spectrum of GO shows several characteristic peaks corresponding to O–H vibration at 3149 cm^{-1}, C=O stretching at 1737 cm^{-1}, C=C skeletal vibration from unoxidized graphitic domains at 1631 cm^{-1}, C–C aromatic ring at 1402 cm^{-1}, C–O

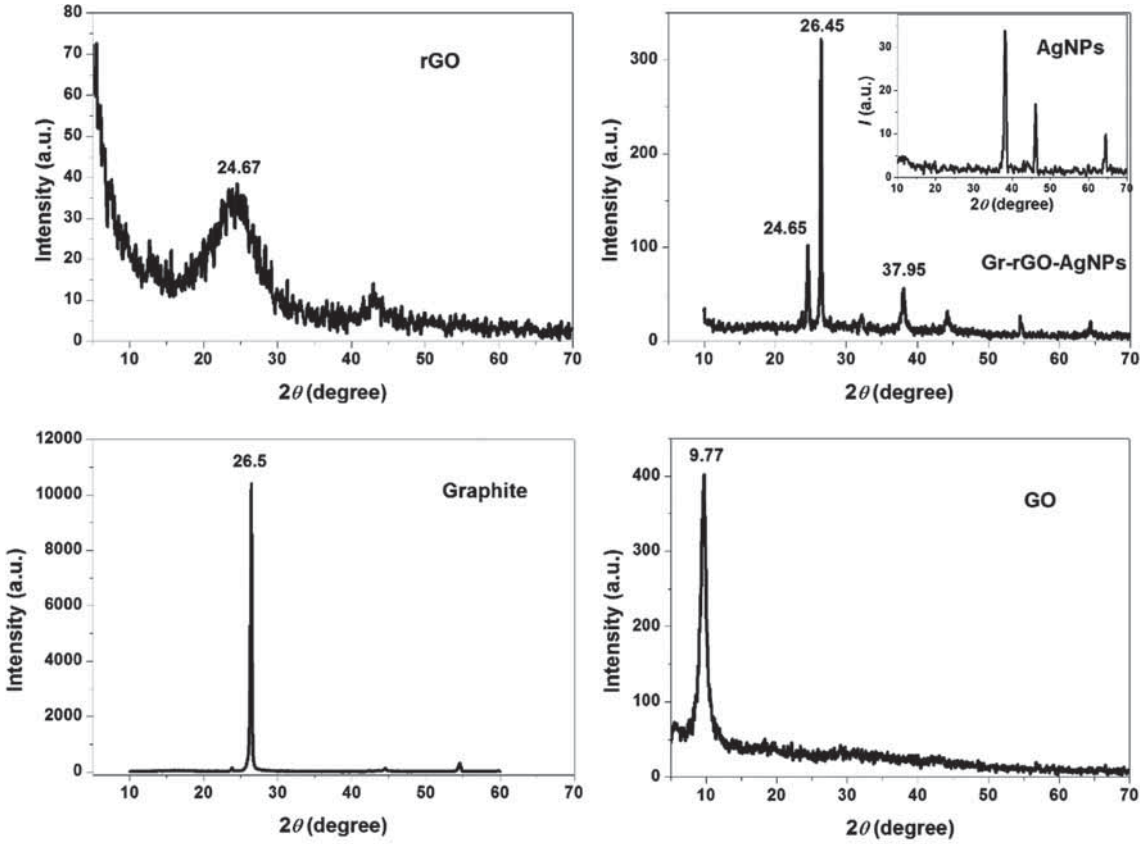

Figure 3. X-ray powder diffractogram of rGO, GO and graphite.

stretching mixed with C–OH bending at 1119 cm^{-1}, and O–H–O out-of-plane wagging at 744 cm^{-1}. After the reduction, the peaks corresponding to C=O stretching at 1737 cm^{-1} disappeared, while the peaks at 1631 (C=C) and 3149 cm^{-1} (OH) were retained. The peak at 1086 cm^{-1} corresponds to C–N stretch. It shows that the reduction results in the formation of sp^2 carbon structure [31]. Thus, rGO sheets were produced via the reduction of GO.

Figure 3 shows the XRD patterns of graphite, GO and rGO. The 2θ diffraction peaks of graphite at 26.543, 44.517 and 54.663° are attributed to the (002), (101) and (004) planes, respectively, corresponding to an interlayer spacing of 0.335 nm. However, it was found that GO exhibited a sharp peak at 9.77° for the (002) plane, and the interplanar spacing increased to 0.904 nm. The D-spacing of GO was larger than graphite due to the introduction of the oxygenated functional groups on carbon sheet, which suggests that graphite was successfully oxidized. After the chemical reduction by hydrazine, the sharp peak of GO disappeared, while another broad peak at around 24.67° for (002) plane was found. The disappearance of the sharp peak could be attributed to the exfoliation of layered structures of GO. The broad peak indicates regeneration of sp^2 carbon bond after undergoing oxidation and deoxidation [32]. In the case of Gr–rGO–AgNPs composite material, the diffraction peaks at 24.65, 26.45 and 37.95° were for the diffraction from (002), (002) and (111) planes of rGO, graphite and face-centred-cubic AgNPs crystal, respectively [26].

Figure 4 illustrates the field emission scanning electron microscopy (FESEM) micrograph of rGO. It displays a well-exfoliated typical wrinkled surface morphology. The geometric wrinkling arises mainly from the defective structure formed by oxygen elimination and from π–π interaction within the sheets of rGO (figure 4a and b). Such structure not only minimizes the surface energy, but also induces mechanical integrity with tensile strength and excellent film-forming ability [33]. It also increases the effective surface to immobilize NPs [32]. The nearly spherical AgNPs with the size range from 50 to 90 nm (figure 4c) were tightly packed on the electrode surface as it is evidenced from the FESEM micrograph of Gr–rGO–AgNPs composite material (figure 4c). A nafion membrane was cast on the rGO–AgNPs immobilized on the surface of the electrode to prevent their leakage from the carbon paste electrode for long-term stability of the sensor [34].

Figure 5a and b shows the TEM micrograph of rGO. It can be seen that rGO has a flake-like layered structure due to the interlayer π–π interaction [35]. Furthermore, the selected area electron diffraction (SAED) as shown in figure 5c, suggests that rGO has good crystalline characteristics

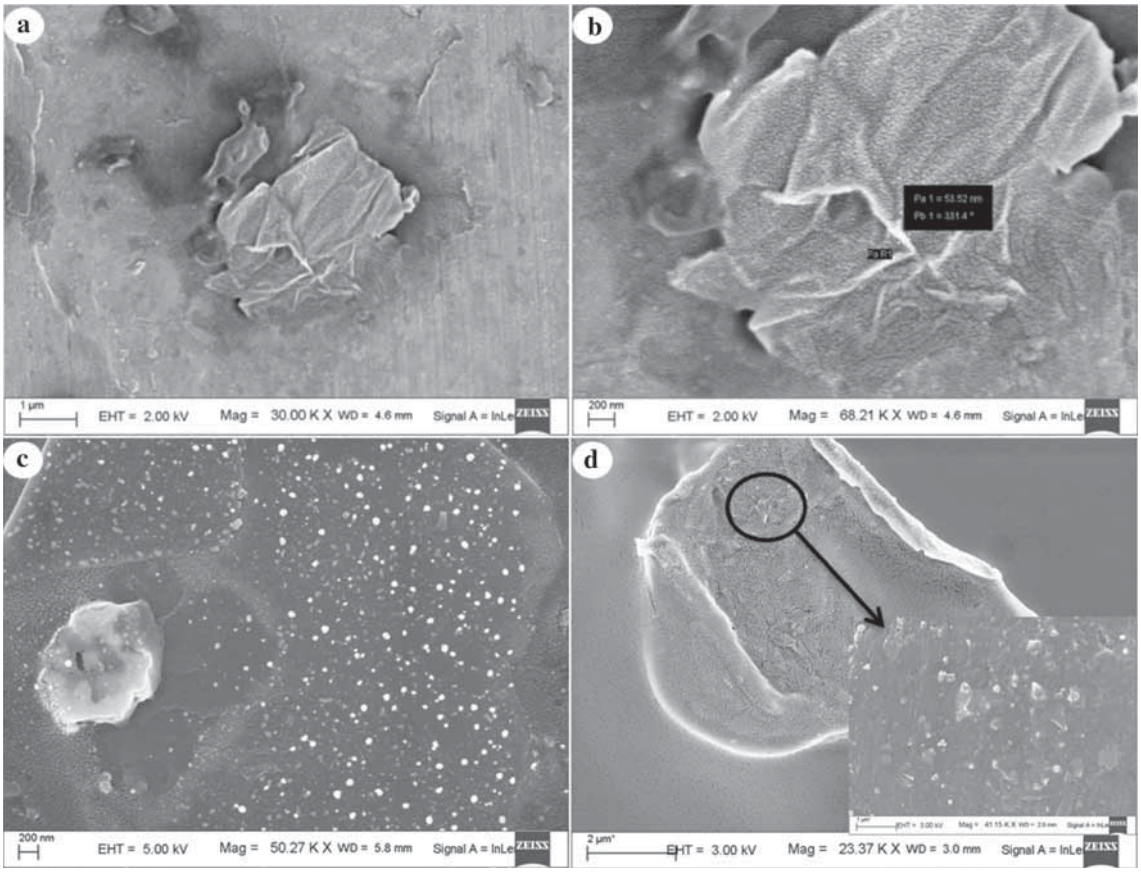

Figure 4. FESEM micrograph of (**a** and **b**) rGO, (**c**) AgNPs and (**d**) Gr–rGO–AgNPs.

[36]. Several sets of sharp hexagonal diffraction patterns are observed. It corresponds to (002) plane of rGO with six brilliant points with a hexagonal symmetry, which is in agreement with the Bragg reflection plane. The high-resolution transmission electron microscopy (HRTEM) micrograph (figure 5d) of rGO sheet showed a clear lattice fringes with an interplanar *d*-spacing of 0.36 nm.

Figure 6 is a typical AFM image of rGO dispersion in water after their deposition on a glass-slide surface through a drop-casting method [33]. The average thickness of as-prepared rGO measured from the height profile of the AFM micrograph (figure 6b), is about 9 nm, even though the most of the oxygen-containing functional groups were removed after the reduction. The particle sizes observed had a diameter ranging from 50 to 90 nm with a mean diameter of 70 nm.

TGA (figure 7) was used to assess the thermal stability of rGO and its precursor. Mass loss below 100°C (∼15%) can be ascribed to the removal of adsorbed water in GO and rGO. GO showed a significant mass loss (30%) between 100 and 200°C indicating CO and CO_2 release from the bulk pyrolysis of the carbon skeleton. Whereas, the steady mass loss between 200 and 800°C amounts to 20% due to the release of more stable oxygen functionalities [37]. In contrast, rGO showed a better thermal stability. The mass loss was some what less at around 200°C due to the removal of thermally labile oxygen functional groups by the reaction of GO with hydrazine. The lower mass loss in the case of rGO at 800°C implies the presence of more stable oxygen functionalities.

3.2 *Cyclic voltammogram (CV) and H_2O_2 sensing*

Figure 8 shows the CV in N_2-saturated 0.2 M phosphate buffer solution at pH 6.74 with an initial amount of 1 mM H_2O_2. No peak was observed in the potential (E_{cat}) range from 0.2 to −0.6 V for graphite working electrode (WE). In the case of Gr–rGO electrode, the cell current was increased notably, but no redox peak was identified. A distinct pair of redox peaks was observed at $E_{cat} = 0.016$ and −0.21 V *vs*. Ag/AgCl with the Gr–rGO–AgNPs electrode. The redox current with Gr–rGO–AgNPs electrode was significantly higher by one–two orders of magnitude than that of the graphite and Gr–rGO WEs [38]. AgNPs could be easily adsorbed on the surface of rGO due to a large surface area to volume ratio. It also provided an excellent catalytic activity for H_2O_2 reduction. From the distinct peak current of Gr–rGO–AgNPs, it could be inferred that H_2O_2 reduction was due to the addition of

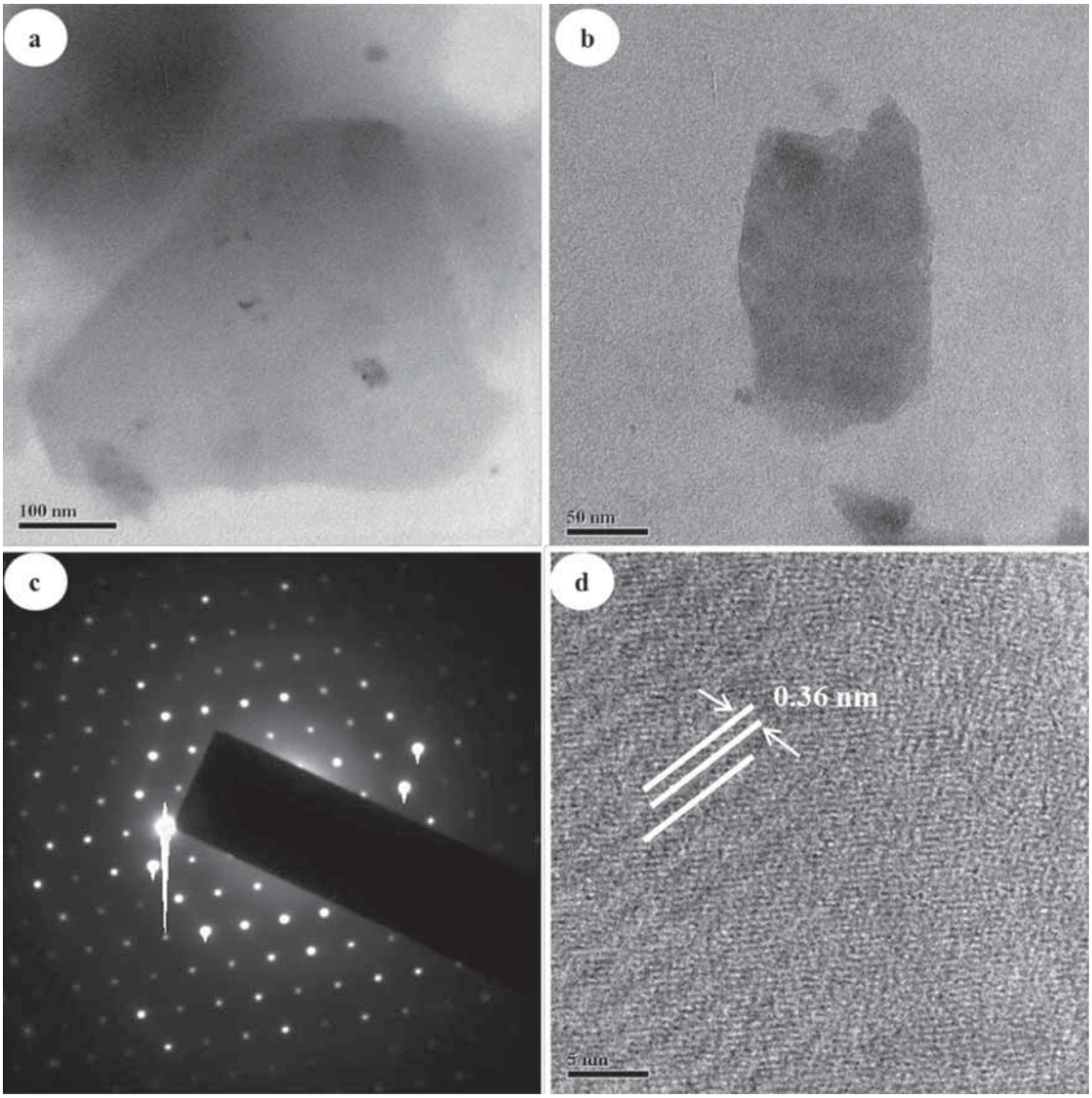

Figure 5. TEM micrograph of (**a**, **b**) rGO, (**c**) SAED of rGO and (**d**) HRTEM micrograph of rGO.

rGO–AgNP nanocomposites, which promote electron transfer and endows electrocatalysis towards H_2O_2 [13]. Moreover, the current at Gr–rGO–AgNPs WE was also enhanced greatly signifying that the rGO nanosheets played a crucial role in performance of the sensor.

Generally, the reduction of H_2O_2 at the graphite electrode takes place as shown in equation (1) [38]. But the reaction is hardly achieved due to a slower electrode kinetics and high overpotential. Interestingly, in the case of Gr–rGO–AgNPs WE, the reduction current was markedly larger than that of the other two WEs due to the different reaction mechanisms (equations (2) and (3)). H_2O_2 is first decomposed into H_2O and O_2, catalysed by AgNPs. Then, the generated O_2 is transported to the surrounding sites, where it is detected by the reduction of O_2 into H_2O_2 [39]. The overpotential was found to be -1.373 V (equation (1)).

$$H_2O_2 + 2e^- + 2H^+ \leftrightarrow 2H_2O \quad (E^0 = -1.583\,\text{V } vs.\ \text{Ag/AgCl}), \tag{1}$$

$$2H_2O_2 \xrightarrow{\text{AgNPs}} O_2 + 2H_2O, \tag{2}$$

$$O_2 + 2e^- + 2H^+ \rightarrow H_2O_2. \tag{3}$$

The amperometric current–time response was used to examine H_2O_2 sensing at Gr–rGO–AgNPs WE. Figure 9a shows the current *vs.* time plots with the successive addition of H_2O_2 in an interval of 50 s. It could be seen that the current responded rapidly achieving the steady-state current within 3 s, and produced a distinct higher current when H_2O_2 was added owing to a faster transport of H_2O_2 molecule from the electrolyte solution to the active sites of the rGO–AgNPs nanocomposite.

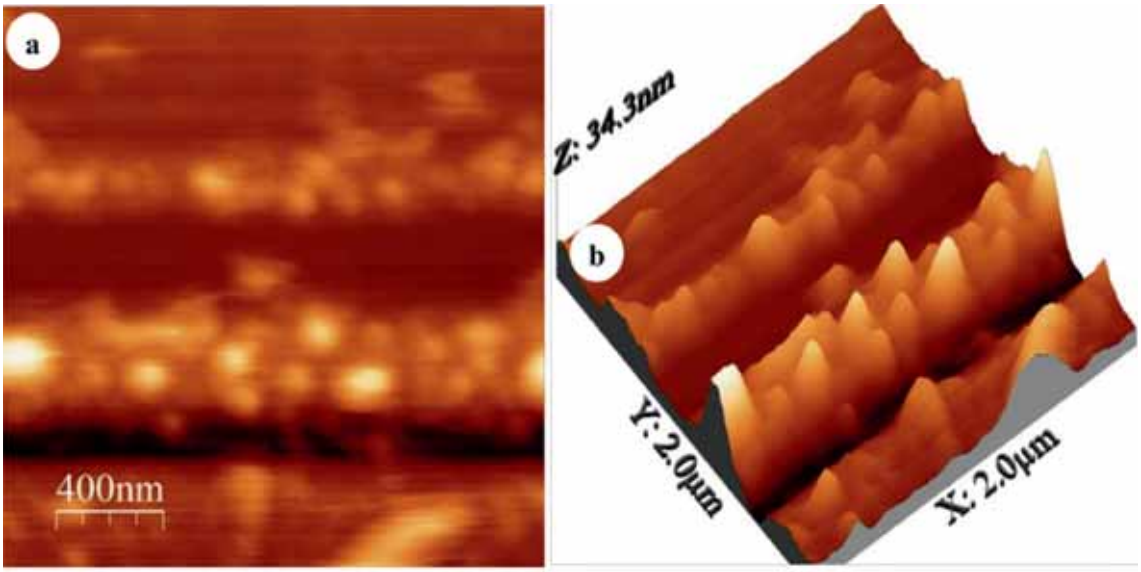

Figure 6. AFM micrographs of rGO: (**a**) 2D and (**b**) 3D.

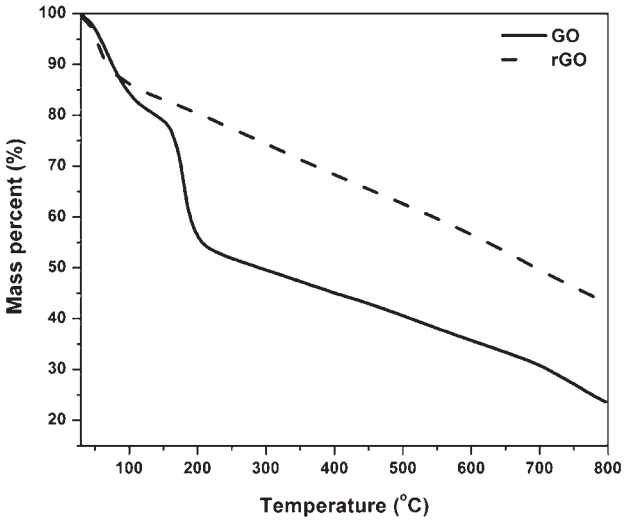

Figure 7. Thermogravimetric analysis (TGA) of GO and rGO.

The corresponding current *vs.* H_2O_2 concentration curve is presented in figure 9b. The current response varied linearly with the addition of H_2O_2, and it weakened gradually when the concentration of H_2O_2 was kept increasing continuously as H_2O_2 bound to most of the catalytic active sites of the electrode at the higher concentration. The linear detection range (R^2 = 0.999) was estimated to be between 1 and 33 mM. The limit of detection (LOD) and the limit of quantification (LOQ) were found to be 19.04 and 57.69 μM, respectively, at a signal to noise ratio of 3. LOD and LOQ were determined using equations (4) and (5), where S_b is the standard deviation determined with 10 blank solutions and b is the slope the analytical curve. Table 1 shows a comparison between the fabricated electrode and the previously reported carbon paste electrodes. Gr–rGO–AgNPs electrode exhibited a comparable potential of H_2O_2 reduction with a high linearity. It implies that the bio-inspired AgNPs are as good as the particles synthesized in a conventional method to provide a faster electron-transfer pathway between H_2O_2 and electrode surface.

$$\text{LOD} = \frac{3.3S_b}{b}, \tag{4}$$

$$\text{LOQ} = \frac{10S_b}{b}. \tag{5}$$

3.3 *Interference and Gr–rGO–AgNPs electrode stability*

The selectivity of the Gr–rGO–AgNPs electrode for the detection of H_2O_2 was also evaluated. Figure 10 shows the current responses in the presence of acetic acid, ascorbic acid, glucose, uric acid, dopamine and ethanol. Gr–rGO–AgNPs exhibited an acceptable selectivity for the electrochemical detection of H_2O_2 as the current response obtained with H_2O_2 did not change with the further addition of 0.1 mM of acetic acid, ascorbic acid, glucose, uric acid, dopamine and ethanol. The interference of common electro-active substances was negligible under the testing condition attributed to a low working potential of Gr–rGO–AgNPs WE [40], and the corresponding cell current variation was <1%. The stability of the sensor was examined by measuring its response to 1 mM H_2O_2 after 10 days. It was found that the sensor retained 98% of its initial current response.

The reproducibility, repeatability and stability of Gr–rGO–AgNPs electrode were investigated. The cell current determined with four fresh Gr–rGO–AgNPs electrodes at

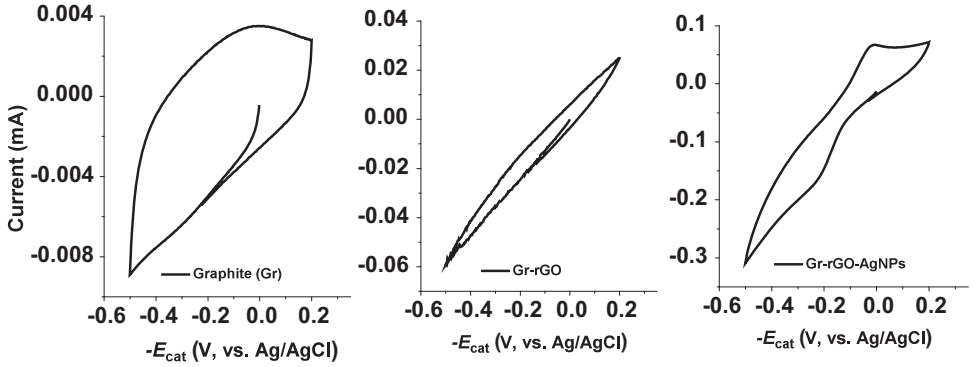

Figure 8. Cyclic voltammogram of unmodified and modified electrodes in N_2 saturated 0.2 M phosphate buffer solution at pH 6.74 in the presence of 1 mM H_2O_2 (scan rate 20 mV s^{-1}).

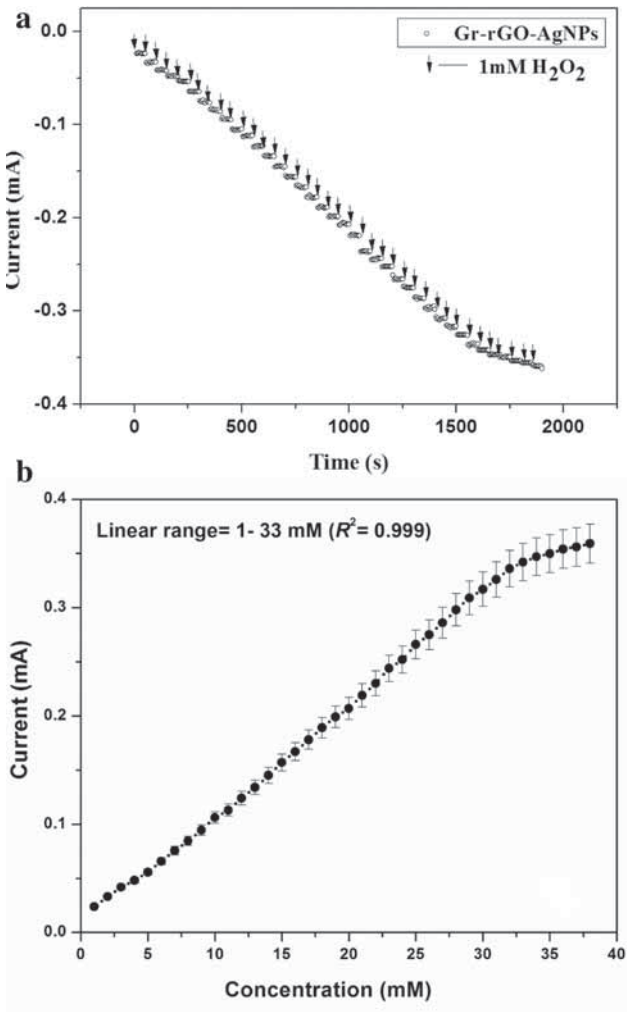

Figure 9. Amperometric response of **(a)** Gr–rGO–AgNPs electrode with successive addition of H_2O_2 in 0.2 M PBS and **(b)** calibration curve at applied potential of −0.21 V *vs*. Ag/AgCl electrode.

$E_{cat} = -0.21$ V *vs*. Ag/AgCl was highly reproducible (relative standard deviation, rsd, 2.43%). The repeatability of the same electrodes was also tested for the detection of 1 mM H_2O_2 for four consecutive runs, and the electrode response was well within rsd of 1.32%. Gr–rGO–AgNPs electrode was stored in open air (average temperature ∼26°C and relative humidity ∼76%) for one month, and the amperometric response was measured with 1mM analyte in PBS at the intervals of 10 days for a period of another one month. It was observed that Gr–rGO–AgNPs electrode could retain 98% of the initial current of the new Gr–rGO–AgNPs electrode after 10 days, and it was 95.3% after 30 days at room temperature.

4. Conclusions

This study was successful for the electrochemical sensing of H_2O_2 at graphite–rGO–AgNPs nanocomposite electrode in the phosphate buffer solution, where AgNPs were synthesized using a green and environmental-friendly technique. The improved Hummer's method was employed for synthesizing GO, which provided a greater amount of hydrophilic oxidized graphene material. Multilayers rGO nanosheet with a thickness of 9 nm synthesized by chemical reduction of GO was evidenced by the Raman shift for the 2D-peak at 2881 cm^{-1} and AFM micrographs. rGO exhibited high crystallinity and thermal stability with 43% mass retention at 800°C. The reduction potential of −0.21 V *vs*. Ag/AgCl with a peak current of 0.165 mA was obtained with the Gr–rGO–AgNPs nanocomposite electrode. However, no distinct potential of H_2O_2 decomposition was noted without AgNPs impregnation i.e., with the graphite–rGO electrode and also the redox current was lower by one order of magnitude. The amperometric response became steady within 3 s from the addition of H_2O_2 and the linearity of the detection limit was found within a very high concentration of H_2O_2 (1–33 mM) with a detection limit of 19.04 μM at a signal to noise ratio of 3. The Gr–rGO–AgNPs electrode was also highly selective towards H_2O_2 detection even in the presence of acetic acid, ascorbic acid, glucose, uric acid, dopamine and ethanol.

Table 1. Comparison of the present study with earlier reports on electrochemical H_2O_2 sensing.

Modified graphene substrate	$-E_{cat}$ (V *vs.* Ag/AgCl)	LOD (μM)	LR (mM)	AR (s)	Source
AgNPs/GN/GCE	−0.3	0.5	0.1–100	<2	Ref. [13]
AgNPs/3DG		14.9	0.03–16.21		Ref. [39]
Graphene/nafion/Azure I/AuNPs/GCE	−0.2	10	0.03–5	<3	Ref. [35]
AgNR–rGO/GCE	−0.2	20.4	0.1–70		Ref. [27]
AgNPs–MWCNT–rGO/GCE	−0.35	0.9	0.1–100	<3	Ref. [41]
(DNA–AgNCs)/graphene/GCE	−0.65	3	0.015–23	<3	Ref. [42]
Graphite/rGO/AgNPs	−0.21	19.04	1–33	<3	Present study

E_{cat}: cathodic potential, LOD: limit of detection, LR: linear range, AR: amperometric response, NPs: nanoparticles, GNs: graphene nanosheets, GCE: glassy carbon electrode, NR: nanorods, 3DG: three-dimensional graphene, rGO: reduced graphene oxide, MWCNT: multi-walled carbon nanotube, DNA–AgNCs: polynucleotide-templated silver nanoclusters.

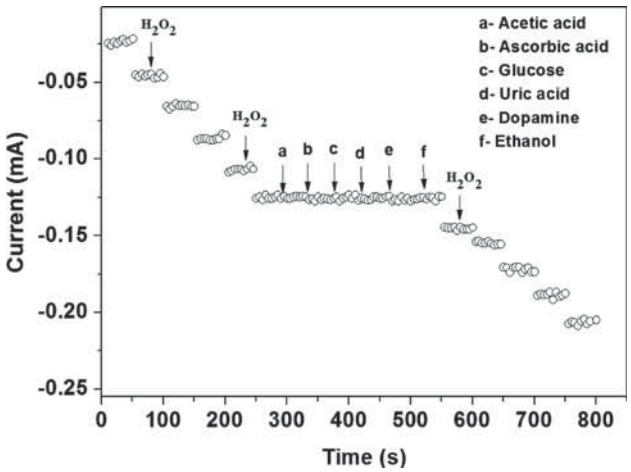

Figure 10. The current response of Gr–rGO–AgNPs electrode for H_2O_2 sensing in the presence of acetic acid, ascorbic acid, glucose, uric acid, dopamine and ethanol.

The amperometric response was high reproducibility (rsd 2.43%) and repeatability (srd 1.32%) after four repeat experiments within a period of one month. The retention of 95.3% of the initial response current after 30 idle days indicates the high stability of the Gr–rGO–AgNPs electrode.

Acknowledgements

We are grateful to the Science & Engineering Research Board, Department of Science and Technology, India, for providing the research Grant (Ref. No. SERC/ET-0343/2012) to this work. We gratefully thank Indian Institute of Technology Guwahati, for providing the necessary research facilities to the Department of Chemical Engineering, and Central Instruments Facility (CIF).

References

[1] Ensafi A A, Jafari-Asl M and Rezaei B 2013 *Talanta* **103** 322
[2] Chen S, Yuan R, Chai Y and Hu F 2013 *Microchim. Acta* **180** 15
[3] Zhou L, Song W, Chen Z and Yin G 2013 *Environ. Sci. Technol.* **47** 3833
[4] Malika M, Rao C V, Das R K, Giri A S and Golder A K 2016 *Appl. Surf. Sci.* **368** 316
[5] Xi F, Zhao D, Wang X and Chen P 2013 *Electrochem. Commun.* **26** 81
[6] Wen F, Dong Y, Feng L, Wang S, Zhang S and Zhang X 2011 *Anal. Chem.* **83** 1193
[7] Luo Y, Liu H, Rui Q and Tian Y 2009 *Anal. Chem.* **81** 3035
[8] Chen S, Yuan R, Chai Y, Zhang L, Wang N and Li X 2007 *Biosens. Bioelectron*. **22** 1268
[9] Yang W, Li Y, Bai Y and Sun C 2006 *Sens. Actuat. B* **115** 42
[10] Bo X, Bai J, Qi B and Guo L 2011 *Biosens. Bioelectron*. **28** 77
[11] Liu M, Liu R and Chen W 2013 *Biosens. Bioelectron*. **45** 206
[12] Sun X, Dong S and Wang E 2004 *Macromolecules* **37** 7105
[13] Liu S, Tian J, Wang L and Sun X 2011 *J. Nanopart. Res*. **13** 4539
[14] Ahmed S, Ahmad M, Swami B L and Ikram S 2016 *J. Adv. Res.* **7** 17
[15] Li X, Xu H, Chen Z S and Chen G 2011 *J. Nanomater.* **2011** 1
[16] Castro L, Blazquez M L, Munoz J A, González F and Ballester F 2013 *IET Nanobiotech.* **7** 1
[17] Gajbhiye M, Kesharwani J, Ingle A, Gade A and Rai M 2009 *Nanomed. Nanotech. Biol. Med.* **5** 382
[18] Chakraborty S, Rao C V, Das R K, Giri A S and Golder A K 2017 *Toxicol. Environ. Chem.* **99** 434
[19] Iravani S 2014 *Int. Sch. Res. Not.* **2014** 1
[20] Zhou S, Xu H, Yuan Q, Shen H, Zhu X, Liu Y *et al* 2016 *ACS Appl. Mater. Interf.* **8** 918
[21] Singh V, Joung D, Zhai L, Das S, Khondaker S I and Seal S 2011 *Prog. Mater. Sci*. **56** 1178
[22] Gan T and Hu S 2011 *Microchim. Acta* **175** 1
[23] Hummers B S W and Offeman E R 1957 *Prep. Graph. Oxide* **208** 1339
[24] Marcano D C, Kosynkin D V, Berlin J M, Sinitskii A, Sun Z, Slesarev A *et al* 2010 *ACS Nano* **4** 4806
[25] Chelli V R, Bag S S and Golder A K 2017 *Environ. Prog. Sustain. Energy* **36** 192
[26] Chelli V R and Golder A K 2016 *RSC Adv*. **6** 95483

[27] Yu B, Feng J, Liu S and Zhang T 2013 *RSC Adv.* **3** 14303
[28] Farahi A, Achak M, El Gaini L, El Mhammedi M A and Bakasse M 2016 *J. Assoc. Arab. Univ. Basic Appl. Sci.* **19** 37
[29] Yang X, Wang L N, Zhou G Z, Sui N, Gu Y and Wan J 2015 *J. Clust. Sci.* **26** 789
[30] Willemse C M, Tlhomelang K, Jahed N, Baker P and Iwuoha E I 2011 *Sensors* **11** 3970
[31] Zhang J J, Yang H, Shen G, Cheng P, Zhang J and Guo S 2010 *Chem. Commun.* **46** 1112
[32] Zhang K, Zhang Y and Wang S 2013 *Sci. Rep.* **3** 3448
[33] Gurunathan S, Han J W and Kim J 2013 *Int. J. Nanomed.* **8** 2719
[34] Hossain M F and Park J Y 2016 *Sci. Rep.* **6** 21009
[35] Zhang Y, Liu Y, He J, Pang P, Gao Y and Hu Q 2013 *Electrochim. Acta* **90** 550
[36] Zhu C, Guo S, Fang Y and Dong S 2010 *ACS Nano* **4** 2429
[37] Paredes J I, Villar-Rodil S, Solis-Fernandez P, Martınez-Alonso A and Tascon J M D 2009 *Langmuir* **25** 5957
[38] Welch C M, Banks C E, Simm A O and Compton R G 2005 *Anal. Bioanal. Chem.* **382** 12
[39] Zhan B, Liu C, Shi H, Li C, Huang L W and Dong X 2014 *Appl. Phys. Lett.* **104** 243704-1
[40] Wang Q and Yun Y 2013 *Microchim. Acta* **180** 261
[41] Lorestani F, Shahnavaz Z, Mn P, Alias Y and Manan N S A 2015 *Sens. Actuat. B* **208** 389
[42] Xia Y, Li W, Wang M, Nie Z, Deng C and Yao S 2013 *Talanta* **107** 55